




TECHNICAL ARTICLE

Study of the Structural and Magnetic Properties of a Novel CoLa/LaH Nanocomposite Material

W.M. GAMAL ^{1,3} ASMAA A.H. EL-BASSUONY,¹ R.S. HAFEZ,¹
and H.K. ABDELSALAM²

1.—Physics Department, Faculty of Science, Cairo University, Giza, Egypt. 2.—Basic Science Department, Higher Institute of Applied Arts 5th Settlement, New Cairo, Egypt. 3.—e-mail: wgamal@sci.cu.edu.eg

A novel nanocomposite consisting of 0.3 cobalt lanthanum nanoferrite/0.7 lanthanum perovskite–hematite nanoparticles (CoLa/LaH) and lanthanum perovskite–hematite nanoparticles (LaH) was synthesized using a simple method. The crystallite size was determined by the X-ray diffraction (XRD) pattern, and the particle size was determined using atomic force microscopy (AFM) to demonstrate that the nano-samples had sizes within the nanoscale range. Fourier transform infrared analysis was utilized to ensure that the nano-samples were formed. By adding CoLa nanoferrite to the LaH nanoparticles, an improvement in magnetic measurements was observed. The saturation magnetization of the CoLa/LaH nanocomposite was 1.1-fold larger than that of LaH. Also, the CoLa/LaH coercivity was 1.7-fold higher than in LaH. Furthermore, the CoLa/LaH nanocomposite displayed a higher operating high frequency of 8.9 GHz, which could be used in an X-band super-high microwave frequency, than the LaH nanoparticles. The LaH nanoparticles, on the other hand, demonstrated a high operating frequency of 8.2 GHz, which could be used in the C-band super-high microwave frequency. No activity was observed for the investigated samples against the tested microorganisms, which was unexpected behavior. Therefore, the investigated nano-samples are interesting for being applied in magnetic targeting and separators, in particular the CoLa/LaH nanocomposite.

INTRODUCTION

Numerous experts are putting much effort into enhancing the physical characteristics of various materials to make them appropriate for various applications.^{1–5} Nanoferrites have generated a great deal of interest over the last decade owing to their wide range of applications, including catalysis, ceramics, magnetism, electricity, and optics.^{6–11} Cobalt nanoferrite, in particular, is a promising nanomaterial due to its mild saturation magnetization, strong coercivity, chemical stability, and significant potential in heavy metal wastewater treatment.^{12–14} Lanthanum perovskite also offers various uses, including photocatalysis, water

splitting, and sensors.^{15,16} Furthermore, hematite nanoparticles are environmentally friendly and efficient nanomaterials, which is important because they may replace harmful anionic surfactants in the samples.^{17,18} To overcome the limitations of employing diverse materials, a revolution in manufacturing nanocomposites has occurred. Additionally, nanocomposites are hybrid/heterogeneous nanomaterials and multi-phase solid materials, created by combining two nanomaterials with various structural and physical characteristics to enhance their distinctive structure and fascinating physical properties for applications, such as UV protection gel, drug delivery, and high-frequency use.¹⁹ The benefits of developing novel nanocomposite materials include enhanced thermal stability and magnetic, electric, and optical characteristics. Incorporating nanocomposite materials into industry may resolve

various difficulties, including biological and non-biological challenges, as well as electronics and vehicle issues.²⁰

Nanocomposites are composites in which one phase has a nanoscale morphology, such as nanoparticles or nanotubes.²⁰ They are multiphasic because they contain multiple phases, and at least one of these phases should have a size between 10 nm and 100 nm. Recent developments in this rapidly evolving field have resulted in the creation of a large number of exciting new materials with unexpected properties. Nanocomposites depend on building blocks with nanoscale dimensions, in order to design and produce innovative materials with remarkable flexibility and enhancement of their physical properties. There are several techniques for creating nanoparticle materials. One of these is the flash auto-combustion technique, which has been used in the current study because it is easy, quick, cost-effective, and saves time, and has piqued the interest of various researchers.^{21–29}

Researchers have developed a wide range of nanocomposite materials by incorporating cobalt nanoferrite with other materials for a wide range of uses.²⁰ However, to the best of the authors' knowledge, this is the first time a nanocomposite of CoLa nanoferrite has been prepared with hematite. Here, nanoparticles of lanthanum, cobalt, and hematite were used to make the nanocomposite material because of their unique properties, especially their magnetic properties. Furthermore, the current work intends to improve the structural and magnetic characteristics of LaH nanoparticles, as well as to evaluate their high-frequency application and antibacterial assessment.

EXPERIMENTAL

Sample Preparation and Characterization

The nano-sample lanthanum perovskite–hematite ($\text{LaFeO}_3\text{-Fe}_2\text{O}_3$) (LaH) was prepared using the flash method, as shown in Fig. 1a. Its starting materials were 0.2165 g lanthanum nitrate, 20.2 g iron III nitrate, 15.015 g urea, and a small amount of distilled water, which were mixed for 30 min in a beaker. The beaker was then placed on a heater at 500 °C until a fine powder was produced, which was ground in an agate mortar for 1 h. Additionally, the cobalt lanthanum nanoferrite ($\text{CoLa}_{0.02}\text{Fe}_{1.98}\text{O}_4$) (CoLa) was prepared using the same method at the same temperature. Its starting materials were 14.551 g cobalt nitrate, 0.433 g lanthanum nitrate, 39.996 g iron III nitrate, and 20.03 g urea. Finally, the 0.3 CoLa/0.7 LaH nanocomposite ($0.3 \text{ CoLa}_{0.02}\text{Fe}_{1.98}\text{O}_4/0.7 \text{ LaFeO}_3\text{-Fe}_2\text{O}_3$) was prepared by adding a stoichiometric ratio of LaH with a concentration of 0.7 to a stoichiometric ratio of CoLa nanoferrite with a concentration of 0.3, and then it was ground in an agate mortar for 1 h. All the apparatus used in the present study are listed in Table I(a).

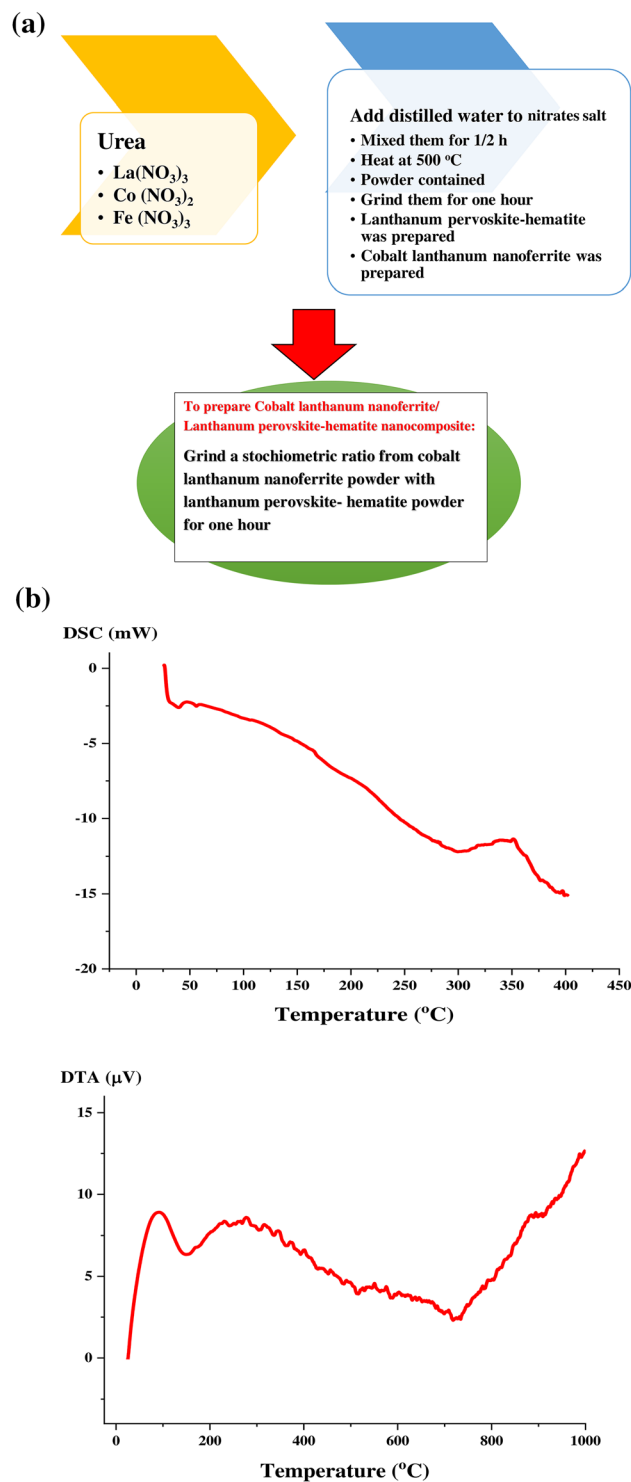


Fig. 1. (a) Preparation method, (b) thermal analyses, (c) XRD analysis, and (d) FTIR spectra of the CoLa/LaH nanocomposite and LaH nanoparticles.

Antimicrobial Measurements

The antimicrobial activities were examined using the modified Kirby–Bauer disk diffusion method.³⁰ The tested bacteria and fungi are described in

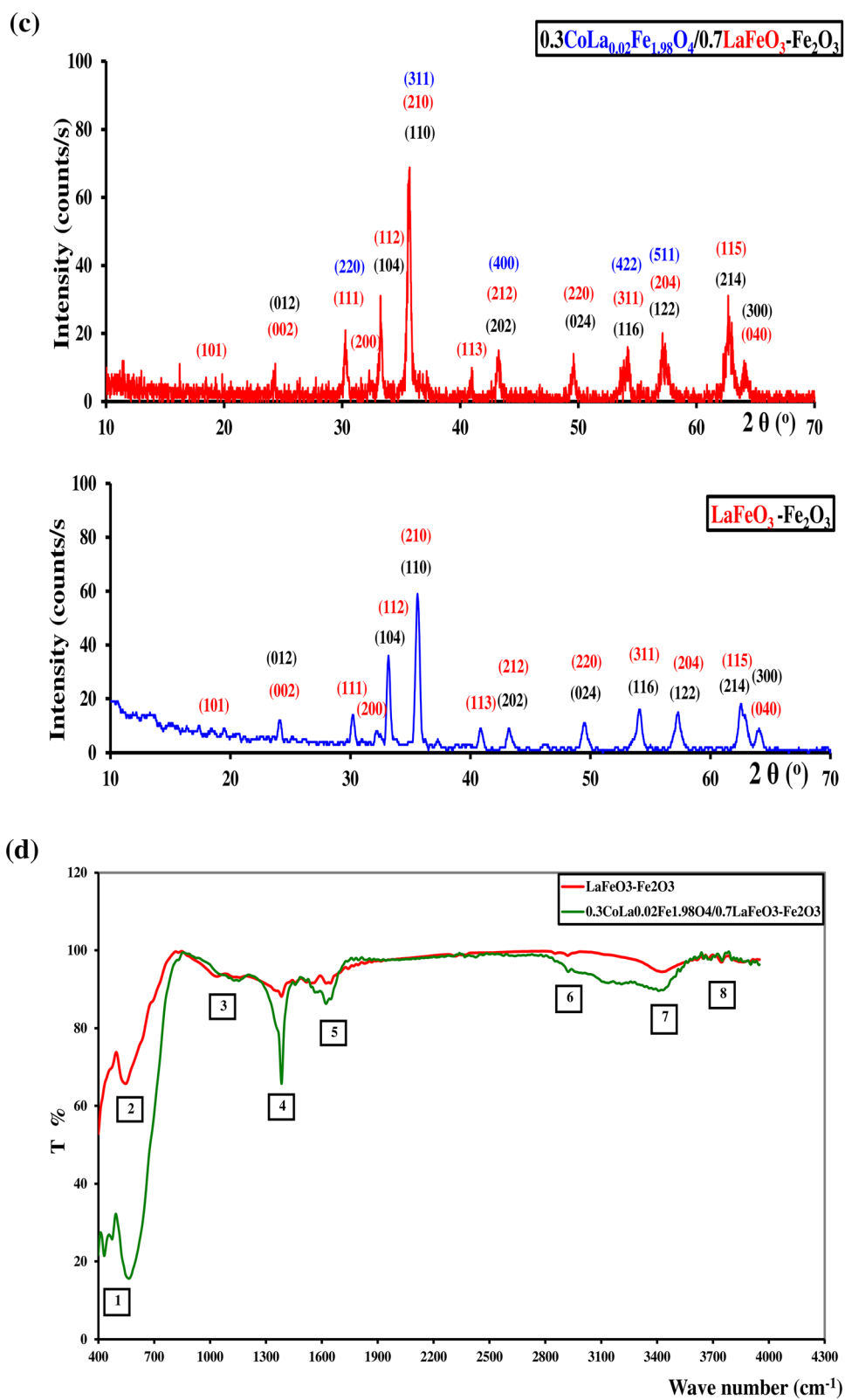


Fig. 1. continued

Table I. (a) Apparatus, and (b) tested microorganism strains used for the CoLa/LaH nanocomposite and LaH nanoparticles analyses

Analysis	Apparatus
(a) <i>Characterization of nanoparticles</i>	
Thermal analyses	NETZSCH STA 409 C/CD
X-ray diffraction pattern (XRD)	Diano Corporation of target CuK α ($\lambda = 1.54 \text{ \AA}$)
Fourier transform infrared (FTIR)	Jasco FTIR 300 E spectrometer
Atomic force microscopy (AFM)	Non-Contact Mode of Wet-SPM-9600
Magnetic measurements	Vibrating sample magnetometer (VSM) model, Lake shore 7410
Type	Micro-organisms/ATCC
(b) <i>Antimicrobial micro-organisms</i>	
Gram-positive bacteria	<i>Bacillus subtilis</i> /6051 <i>Staphylococcus aureus</i> /12600 <i>Streptococcus faecalis</i> /19433 <i>Escherichia coli</i> /11775
Gram-negative bacteria	<i>Neisseria gonorrhoeae</i> /19424 <i>Pseudomonas aeruginosa</i> /10145
Fungi	<i>Candida albicans</i> /7102 <i>Aspergillus flavus</i> /9643

Table II. Crystallite size, particle size, and roughness of the CoLa/LaH nanocomposite and LaH nanoparticles

Sample	Crystallite size (nm)	Particle size AFM (nm)	Roughness
LaFeO ₃ -Fe ₂ O ₃	26.3	75.95	1.420
0.3CoLa _{0.02} Fe _{1.98} O ₄ /0.7LaFeO ₃ -Fe ₂ O ₃	27.7	164.4	1.423

Table III. FTIR peaks of the CoLa/LaH nanocomposite and LaH nanoparticles

No. of peaks	1	2	3	4	5	6	7	8
LaFeO ₃ -Fe ₂ O ₃	402.1	545.8	1156.01	1382.7	1645.9	2919.7	3424.9	3746.1
0.3CoLa _{0.02} Fe _{1.98} O ₄ /0.7LaFeO ₃ -Fe ₂ O ₃	431.01	565.04	1154.2	1383.7	1621.8	2922.6	3408.6	3748.9

Table I(b). The investigated samples were examined on 100 μ L of the tested bacteria and fungi in vitro, which were grown in 10 mL of fresh media until the bacteria count was 10^7 cells/mL and the fungi count 10^5 cells/mL. The samples were incubated at 30 °C for 24–48 h. Finally, the inhibition zone diameters were measured.

RESULTS AND DISCUSSION

Thermal Analyses

The differential scanning calorimetry (DSC) and differential thermal analysis (DTA) of LaFeO₃-

Fe₂O₃ (lanthanum perovskite-hematite) (LaH) nanoparticles are shown in Fig. 1b. The DSC graph reveals two peaks, one endothermic at 25 °C due to water loss and one exothermic at 300–375 °C due to metal nitrate combustion with urea.³¹ As a result, the formation temperature of the studied sample was over 400 °C. As a consequence, the nano-sample was prepared at 500 °C. The DTA curve for the investigated material reveals two peaks. The first peak (100–200 °C) was endothermic due to water loss. The second endothermic peak occurred at 700 °C due to the enhanced crystallization of the material at this annealing temperature.

XRD Study

The X-ray diffraction (XRD) pattern for LaH nanoparticles and CoLa/LaH nanocomposite is shown in Fig. 1c, and depicts a multi-phase structure for both samples, which were assigned ICDD card numbers (01-082-3106) for lanthanum perovskite (LaFeO_3), (04-006-8177) for hematite (Fe_2O_3), and (04-005-7078) for cobalt lanthanum nanoferrite. Using the Debye–Scherrer equation,³² the crystallite sizes of the studied materials were determined, and their values are shown in Table II:

$$D = \frac{K\lambda}{B \cos \theta}, \quad (1)$$

where B is the full width of half maximum, K is the shape factor = 0.9, and λ is the wavelength of $\text{CuK}\alpha$ radiation = 1.54 Å. The broadness of the XRD peaks, as shown in Fig. 1c and Table II, corresponds to lower crystallite sizes for the LaH nanoparticles compared with the CoLa/LaH nanocomposite. Finally, the XRD analysis confirmed the formation of the samples.

FTIR Study

The Fourier transform infrared (FTIR) spectra of the LaH and CoLa/LaH nanocomposites are shown in Fig. 1d, and the data are presented in Table III. Eight peaks in the FTIR spectra of both materials are found: two (peaks 1 and 2) are strong bands

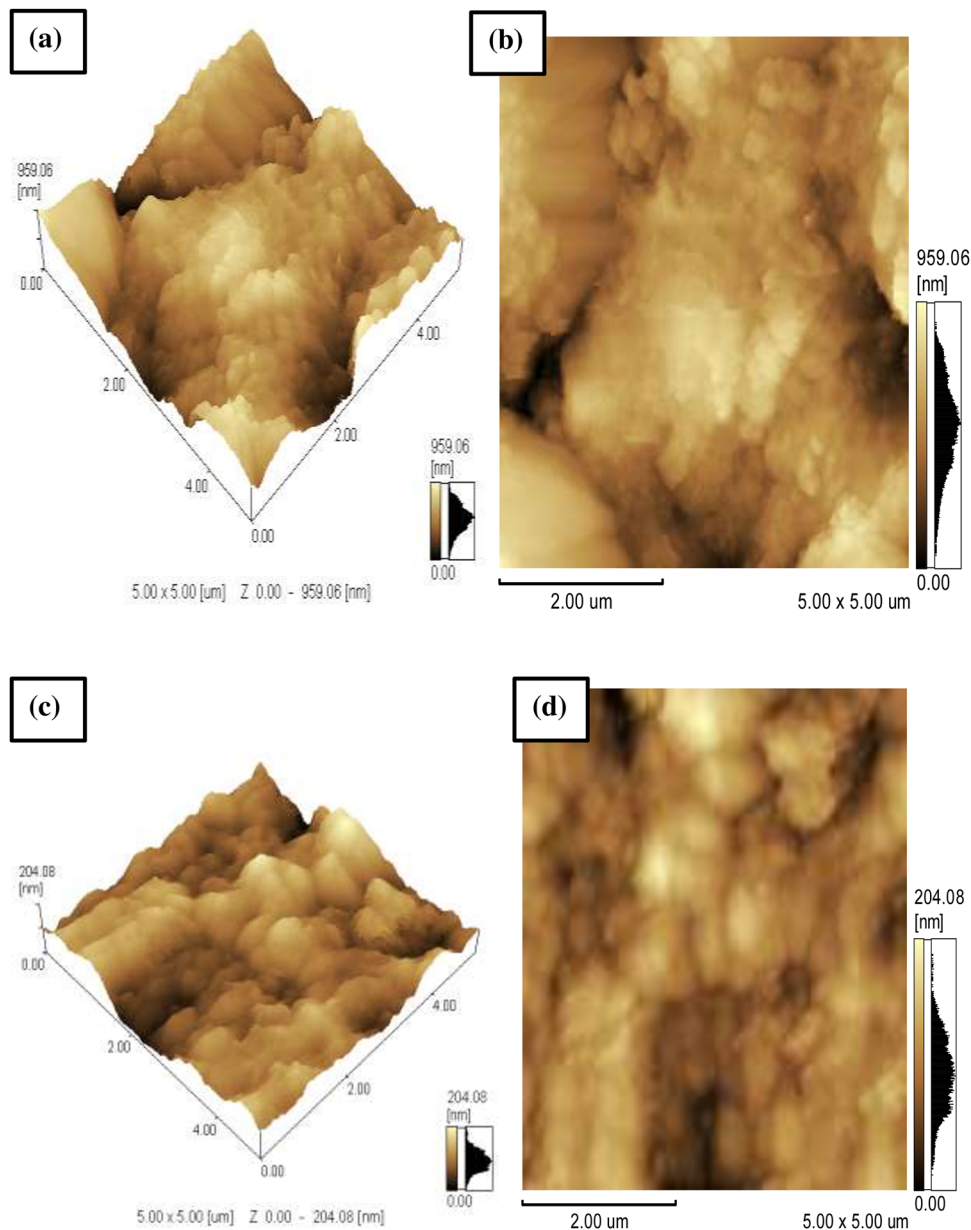


Fig. 2. (a) AFM micrograph and plane image, and (b) the average particle size and roughness of the LaH nanoparticles and CoLa/LaH nanocomposite.

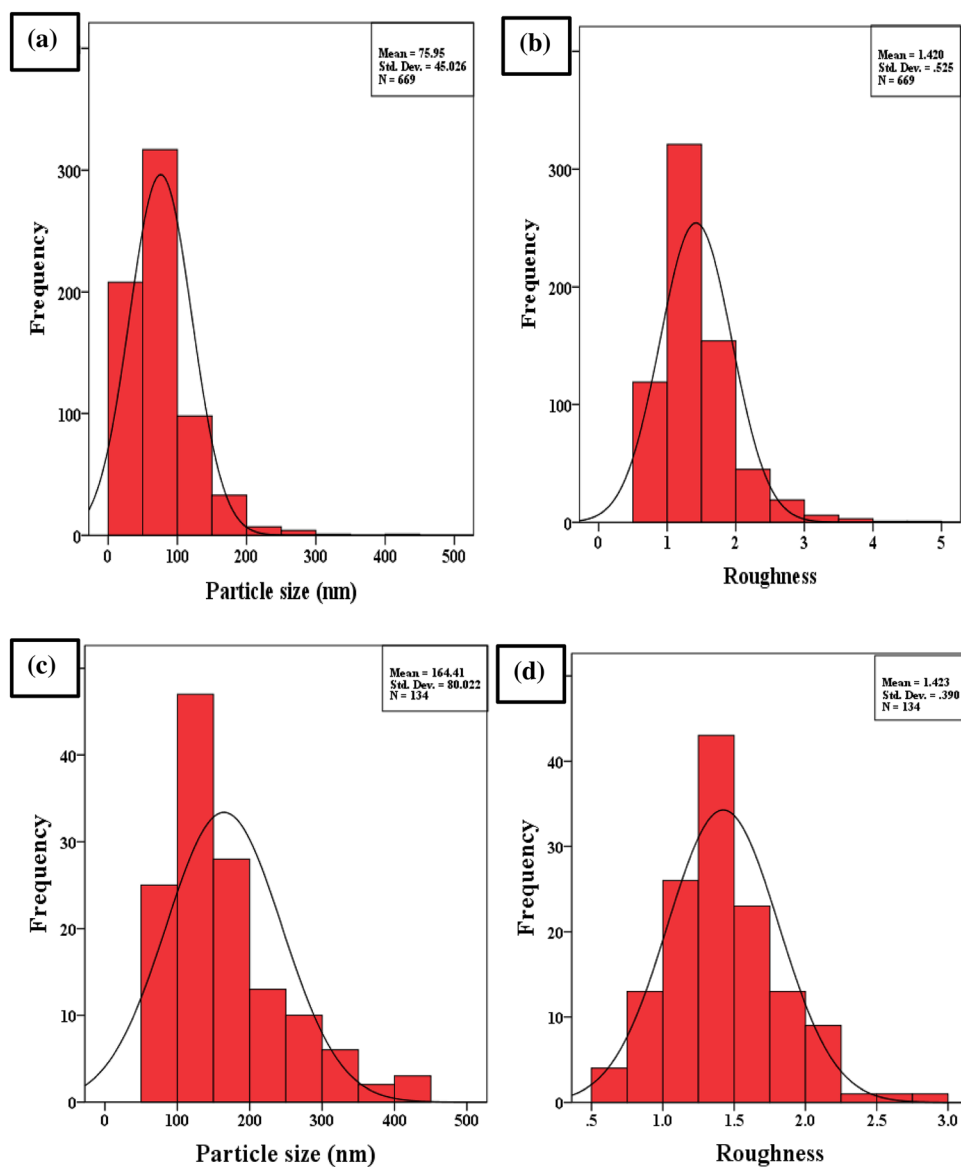


Fig. 2. continued

usually seen in all ferrites for the octahedral and tetrahedral sites.³³ When CoLa nanoferrite is added to LaH nanoparticles, most peaks exhibit a minor shift to high frequency, because the metal–oxygen band position is responsible for this alteration. The stretching vibration of peak 3 is assigned to the C–O–C group. However, peak 4 is attributable to the usage of metal nitrate during manufacture. The carboxyl group is responsible for the stretching vibration of peak 5. The band at peak 6 represents the OH group, while the bands at peaks 7 and 8 represent the CH and NH groups, respectively. Consequently, all the previous FTIR analysis peaks indicate the creation of the nano-samples.

AFM Study

Figure 2(a: a, b, and c, d) shows the atomic force microscopy micrograph (AFM) for the LaH nanoparticles and the CoLa/LaH nanocomposite, respectively. The images represent small particles (75.9–164.4 nm) with a cluster owing to the lack of surfactants during synthesis, such as polyvinyl alcohol. In addition, the agglomeration is minor, due to the presence of hematite in the sample's composition.^{34,35} Figure 2b shows the average particle size (75.9–164.4 nm) and the roughness (1.420–1.423 μm) of the LaH nanoparticles (Fig. 2b: a, b) and the CoLa/LaH nanocomposite (Fig. 2b: c, d) using the IBM SPSS Statistics 22 program, and the values are reported in Table II. The CoLa/LaH

nanocomposite has a slightly greater roughness (1.420–1.423 μm) than LaH nanoparticles, because the particle size is greater than that of the LaH nanoparticles. The average particle size (75.9–164.4 nm) is larger than the crystallite size (26.3–27.7 nm) provided in Table II, due to the particle size being a cluster of tiny crystallites.³⁶ Finally, the average particle size and crystallite size from the XRD examination of the samples emphasizes that the nano-samples' sizes are in the nanoscale range.

Magnetic Study

Figure 3a depicts the magnetic hysteresis loop for the LaH nanoparticles and the CoLa/LaH nanocomposite at 300 K. The samples' hysteresis loop reveals soft ferromagnetism. By adding the CoLa nanoferrite to the LaH nanoparticles, all the magnetic parameters for the CoLa/LaH nanocomposite increased by a factor of 1.7 for coercivity (H_c), 1.3 for remnant magnetization (M_r), 1.1 for saturation magnetization (M_s), and 1.2 for squareness (R), as shown in Table IV. The inclusion of a small concentration of cobalt nanomaterial, known as a hard ferrite, increases the coercivity of the CoLa/LaH nanocomposite by 1.7-fold when compared to the LaH nanoparticles. In addition, this increase is the result of a 1.8-fold increase in the

magnetocrystalline anisotropy constant (k) of the CoLa/LaH nanocomposite compared to that of the LaH nanoparticles, computed as follows:^{37–40}

$$k = \frac{M_s H_c}{0.98} \quad (2)$$

Generally, it is necessary to measure the nano-sample's squareness to determine the nanoparticles' interaction type.^{41,42} The type of interaction between the nanoparticles in this work was a magnetostatic interaction, with $R = 0.5$, which is estimated by:^{43,44}

$$R = \frac{M_r}{M_s} \quad (3)$$

Figure 3b illustrates the first derivative of the magnetization concerning the applied field (magnetic susceptibility $\chi = dM/dH$) for the materials, and Table IV lists the results. Both samples displayed a high magnetic susceptibility, χ , due to their high saturation magnetization, M_s . This is a significant finding that makes the materials, particularly the CoLa/LaH nanocomposite, applicable as a magnetic target and separator. The figure also illustrates that the CoLa/LaH nanocomposite has a broader width than the LaH nanoparticles owing to a 1.7-fold increase in coercivity of the CoLa/LaH

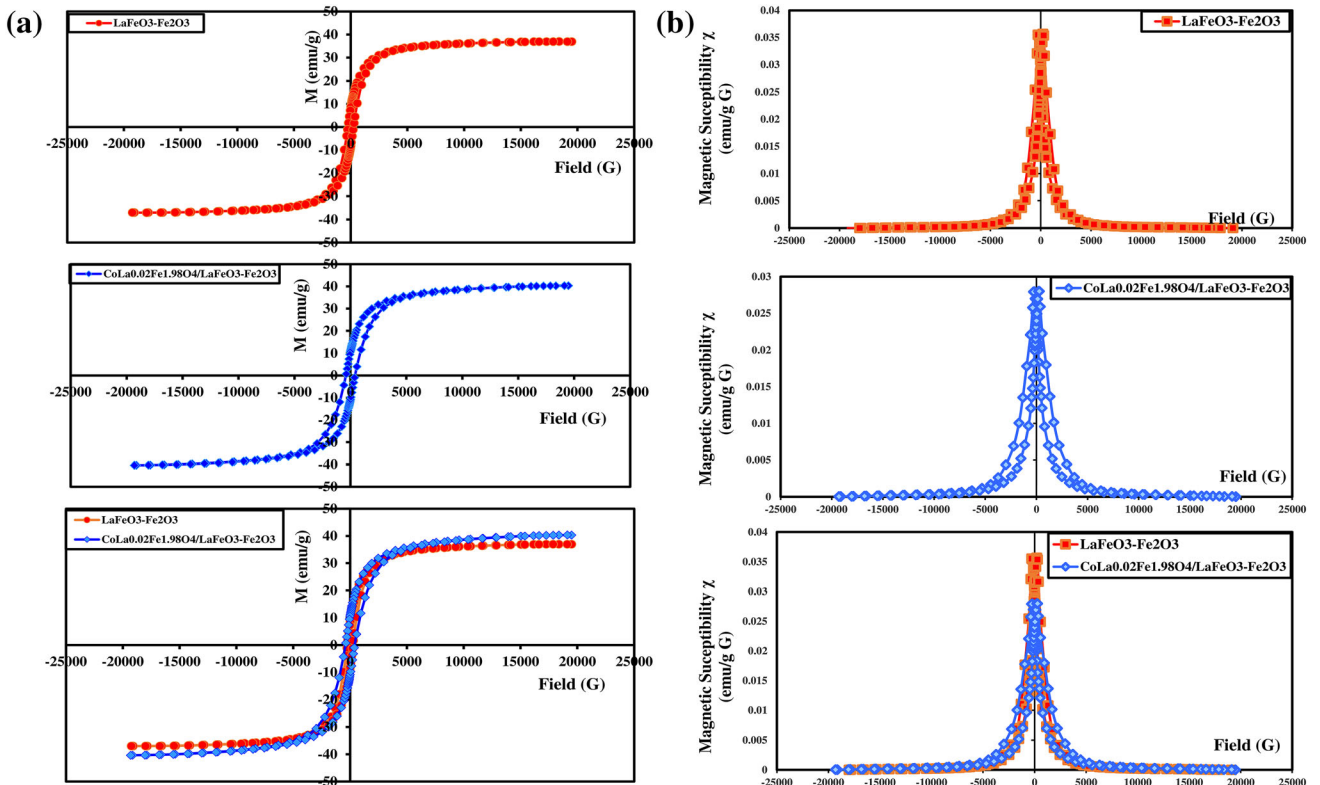


Fig. 3. (a) Magnetic hysteresis loop, (b) magnetic susceptibility, and (c) operating high frequency of the CoLa/LaH nanocomposite and LaH nanoparticles.

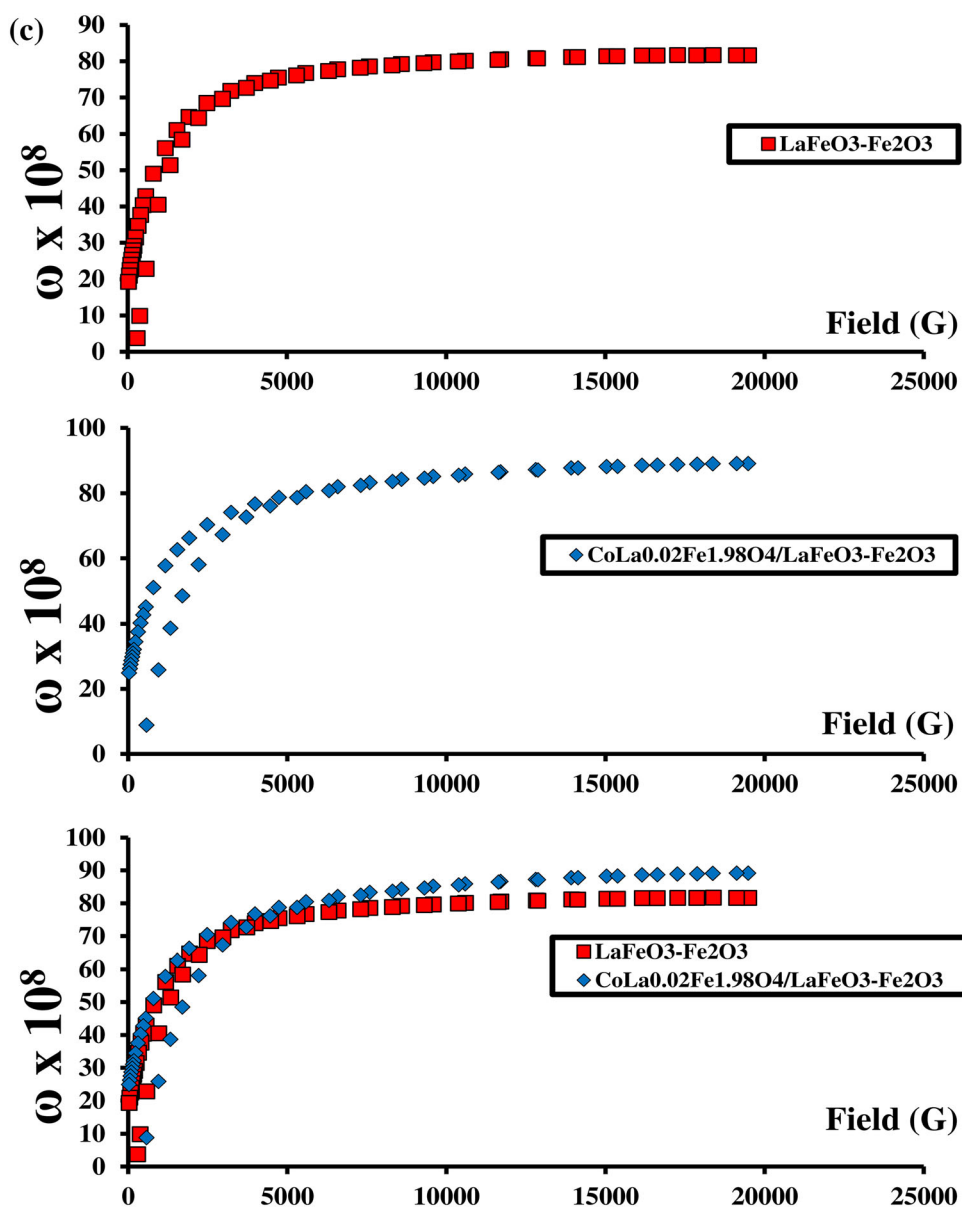


Fig. 3. continued

Table IV. Magnetic parameters of the CoLa/LaH nanocomposite and LaH nanoparticles

Magnetic parameters	H_c (G)	M_s (emu/g)	M_r (emu/g)	Squareness (M_r/M_s)	Magnetocrystalline anisotropy constant k (erg/g)	Magnetic susceptibility χ^2 (emu/g. G) $\times 10^{-2}$	ω (GHz)
LaFeO ₃ -Fe ₂ O ₃	242.33	36.977	8.1818	0.2213	9143.5	3.57	8.2
0.3CoLa _{0.02} Fe _{1.98} O ₄ /0.7LaFeO ₃ -Fe ₂ O ₃	403.77	40.353	10.786	0.26731	16,293.3	2.70	8.9

nanocomposite. Consequently, adding CoLa to the LaH nanoparticles improved their magnetic characteristics, allowing them to be used in magnetic targeting and separation.

High-Frequency Application

The ranges of operational frequency values (30–300 MHz for radio waves and 300 MHz to 300 GHz

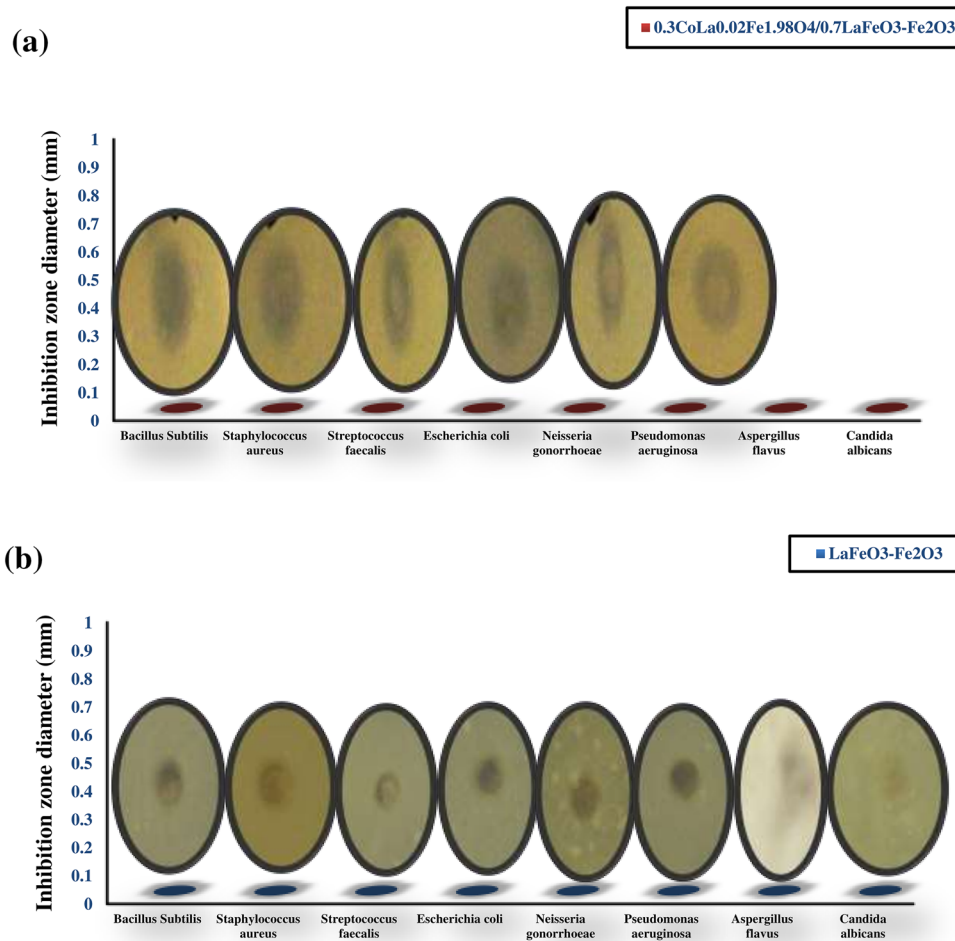


Fig. 4. Antimicrobial activities of the (a) CoLa/LaH nanocomposite, and (b) LaH nanoparticles.

for microwaves) are essential for developing high-performance high-frequency devices.⁴⁵ Figure 3c depicts the high operating frequency for the LaH nanoparticles and CoLa/LaH nanocomposite, and Table IV lists the results. The high operating frequency was determined by:⁴⁶

$$\omega = 8\pi^2\gamma M, \quad (4)$$

where γ and M represent the gyromagnetic ratio, $\gamma = 2.8$ MHz/G, and the magnetization, respectively. Both samples showed high-frequency ranges due to their high saturation magnetization, as illustrated in Fig. 3b and Table IV. The LaH nanoparticles have a frequency of 8.2 GHz, allowing them to be used in the very high microwave frequency C-band, whereas the CoLa/LaH nanocomposite demonstrated a value of 8.9 GHz, allowing it to be used in the very high microwave frequency X-band. Finally, the samples exhibited fascinating microwave frequency applications.

Antimicrobial Study

The antimicrobial properties were studied for both samples. Figure 4a and b depicts the in vitro antibacterial activity of the samples. In previous studies, each of the LaFeO₃ and Fe₂O₃ nanoparticles has shown strong antibacterial activities.^{47–49} Conversely, in the current research, they omit their activity, which is referred to as the antagonistic impact when combined. According to the findings of the antimicrobial investigation, neither sample had any impact on the Gram-positive and Gram-negative bacteria and fungi that were examined. This was due to the nano-samples' antagonistic impact on the bacteria and fungi, which was unexpected.⁵⁰ Therefore, introducing strong antibacterial substances did not affect the microorganisms.^{51–53}

CONCLUSION

Lanthanum perovskite-hematite (LaFeO₃-Fe₂O₃) (LaH) nanoparticles and a cobalt lanthanum nanofer-

rite/lanthanum perovskite-hematite (0.3CoLa_{0.02}Fe_{1.98}O₄/0.7LaFeO₃-Fe₂O₃) (CoLa/LaH) nanocomposite were prepared using a rapid method (flash). The XRD and AFM investigations of structure and morphology revealed that the materials have nanoscale sizes. The CoLa/LaH nanocomposite exhibited a greater saturation magnetism than the LaH nanoparticles, allowing its use in magnetic targeting and separators. In addition, the nanocomposite (CoLa/LaH) demonstrated a high operating frequency for use in X-band ultra-high microwave frequency applications. The LaH nanoparticles, on the other hand, demonstrated a lower frequency than the CoLa/LaH nanocomposite, which allowed their application in the C-band super high microwave frequency. The antibacterial properties were investigated, but no activity was detected against the tested bacteria and fungi. Finally, the magnetic characteristics of the LaH nanoparticles were improved by adding a small concentration (0.3) of CoLa nanoferrite, allowing them to be used in various applications.

FUNDING

Open access funding provided by The Science, Technology & Innovation Funding Authority (STDF) in cooperation with The Egyptian Knowledge Bank (EKB).

CONFLICT OF INTEREST

The authors declare that they have no conflict of interest.

HUMAN AND ANIMAL RIGHTS

This article does not contain any studies with human or animal subjects.

OPEN ACCESS

This article is licensed under a Creative Commons Attribution 4.0 International License, which permits use, sharing, adaptation, distribution and reproduction in any medium or format, as long as you give appropriate credit to the original author(s) and the source, provide a link to the Creative Commons licence, and indicate if changes were made. The images or other third party material in this article are included in the article's Creative Commons licence, unless indicated otherwise in a credit line to the material. If material is not included in the article's Creative Commons licence and your intended use is not permitted by statutory regulation or exceeds the permitted use, you will need to obtain permission directly from the copyright holder. To view a copy of this licence, visit <http://creativecommons.org/licenses/by/4.0/>.

REFERENCES

- H. Li, Q. Chen, J. Zhao, and K. Urmila, *Sci. Rep.* 5, 11033 (2015).
- E.S. Anooj, S.J. Sreelekshmi, S.T. Gopukumar, and P.K. Praseetha, *Int. J. Pharm. Sci. Rev. Res.* 46, 22 (2017).
- N.A. Kaskhedikar and J. Maier, *Adv. Mater.* 21, 2664 (2009).
- C. Shan, Z. Ma, and M. Tong, *J. Hazard. Mater.* 268, 229 (2014).
- M.G. Naseri, E.B. Saion, H.A. Ahangar, and A.H. Shaari, *Mater. Res. Bull.* 48, 1439 (2013).
- G. Nangmenyi, X. Li, S. Mehrabi, E. Mintz, and J. Economy, *Mater. Lett.* 65, 1191 (2011).
- L. Ajroudi, N. Mliki, L. Bessais, V. Madigou, S. Villain, and Ch. Leroux, *Mater. Res. Bull.* 59, 49 (2014).
- D.H.K. Reddy and Y.S. Yun, *Coord. Chem. Rev.* 315, 90 (2016).
- A. Virden, S. Wells, and K. O'Grady, *J. Magn. Magn. Mater.* 316, e768 (2007).
- S. Honary, K. Ghajar, P. Khazaeli, and P. Schalchian, *Trop. J. Pharm. Res.* 10, 69 (2011).
- E. Ateia and A.A.H. El-Bassuony, *J. Mater. Sci. Mater. Electron.* 28, 11482 (2017).
- M.A. Albalah, Y.A. Alsabah, D.E. Mustafa, and S.N. Appl, *Science* 2, 804 (2020).
- M.A. Barakat, *Arab. J. Chem.* 4, 361 (2011).
- P. Shao, J. Tian, X. Duan, Y. Yang, W. Shi, X. Luo, F. Cui, S. Luo, and S. Wang, *Chem. Eng. J.* 359, 79 (2019).
- P. Song, H. Quin, L. Zhang, K. An, Z. Lin, J. Hu, and M. Jiang, *Sens. Actuators B* 310, 312 (2005).
- I.M. Nassar, S. Wu, L. Li, and X. Li, *Chem. Select* 3, 968 (2018).
- M. Hua, S.J. Zhang, B.B. Pan, W.M. Zhang, L. Lv, and Q.X. Zhang, *J. Hazard. Mater.* 211, 317 (2012).
- N. Arjun, G.T. Pan, and T.C.K. Yang, *Results Phys.* 7, 920 (2017).
- X. Liu and M. Antonietti, *Carbon* 69, 460 (2014).
- A.A.H. El-Bassuony, W.M. Gamal, and H.K. Abdelsalam, *J. Mater. Sci. Mater. Electron.* 33, 16219 (2022).
- A.M.A. Henaish, et al., *J. Phys. Conf. Ser.* 1253, 012025 (2019).
- M. Henaish, O.M. Hemedda, A. Alqarni, D.E. El Refaay, Sh. Mohamed, and M.A. Hamad, *Appl. Phys. A* 126, 834 (2020).
- K.S. Al-Namshah, M.F.A. Ibrahim, and M.S. Hamdy, *Physica B* 625, 413459 (2022).
- K.P. Thummer, M.C. Chhantbar, K.B. Modi, G.J. Balda, and H.H. Joshi, *Mater. Lett.* 58, 2248 (2004).
- Y. Ichiyonagi, H. Kondoh, T. Yokoyama, K. Okamoto, K. Nagai, and T. Ohta, *Chem. Phys. Lett.* 379, 345 (2003).
- E.A. Arrasheed, Y.A. Alibwaini, T.M. Meaz, R.M. Shalaby, B.I. Salem, A.W. Ajlouni, H.H. El-Bahnasawy, O.M. Hemedda, and A.M.A. Henaish, *J. Mol. Struct.* 1245, 131273 (2021).
- L.C. Li, J. Jiang, and F. Xu, *Mater. Lett.* 61, 1091 (2007).
- M. Henaish, M. Mostafa, B.I. Salem, H.M.H. Zakaly, S.A.M. Issa, I.A. Weinstein, and O.M. Hemedda, *J. Mater. Sci. Mater. Electron.* 31, 20210 (2020).
- K.S. Rao, A.M. Kumar, M.C. Varma, G.S.V.R.K. Choudary, and K.H. Rao, *J. Alloys Compd.* 488, L6 (2009).
- A.W. Bauer, W.M. Kirby, C. Sherris, and M. Turck, *Am. J. Clin. Pathol.* 45, 493 (1966).
- X. Ning, Z. Xiong, B. Yang, W. Lu, and S. Wu, *Catalysts* 10, 314 (2020).
- M.A. Sayed, T.M.A. Abd El-Rahman, H.K. Abdelsalam, A.M. Ali, M.M. Hamdy, Y.A. Badr, N.H. Abd El-Rahman, S.M. Abd El-Latif, S.H. Mostafa, S.S. Mohamed, Z.M. Ali, and A.A.H. El-Bassuony, *BMC Chem.* 16, 39 (2022).
- R.D. Waldron, *Phys. Rev.* 99, 1727 (1955).
- Y. Yu, J. Peng, B. Liu, G. Chen, and C. Srinivasakannan, *High Temp. Mater. Proc.* 32, 303 (2013).
- P.C. Nagajothi, P. Muthuramanb, T.V.M. Sreekanthc, D.H. Kimb, and J. Shim, *Arab. J. Chem.* 10, 215 (2017).
- Z. Ye, Z. Deng, L. Zhang, J. Chen, G. Wang, and Z. Wu, *Mater. Res. Express* 7, 035007 (2020).

37. B.B. Straumal, S.G. Protasova, A.A. Mazilkin, E. Goering, B. Baretzky, and P.B. Straumal, *Jetp Lett.* 97, 367 (2013).
38. S. Mørup, M.F. Hansen, and C. Frandsen, *Compr. Nanosci. Technol.* 1, 437 (2011).
39. M. Mahmoudi, S. Sant, B. Wang, S. Laurent, and T. Sen, *Adv. Drug Deliv. Rev.* 63, 24 (2011).
40. A.A.H. El-Bassuony and H.K. Abdelsalam, *JOM* 71, 1866 (2019).
41. N. Sivakumar, A. Narayanasamy, K. Shinoda, C.N. Chin-nasamy, B. Jeyadevan, and J.M. Greneche, *J. Appl. Phys.* 102, 13916 (2007).
42. M.S. Haque, M.F. Rahman, M.M. Zaman, M.A. Matin, A.K.M.A. Hakim, and M.F. Islam, *Appl. Mech. Mater.* 860, 87 (2016).
43. S.D. Ali, S.T. Hussain, and S.R. Gilani, *Appl. Surf. Sci.* 271, 118 (2013).
44. H.N. Abdelhamid, A. Talib, and H.F. Wu, *RSC Adv.* 5, 34594 (2015).
45. M.N. Akhtar, M. Saleem, and M.A. Khan, *J. Phys. Chem. Solids* 123, 260 (2018).
46. P. Akhtar, M.N. Akhtar, M.A. Baqir, A. Ahmad, M.U. Khallidoon, M. Farhan, and M. Azhar Khan, *J. Mater. Sci. Mater. Electron.* 32, 7692 (2021).
47. C. Singh and M. Rakesh, *Int. J. Chem Tech Res.* 12, 87 (2019).
48. M. Arakha, S. Pal, D. Samantarrai, T.K. Panigrahi, B.C. Mallick, K. Pramanik, B. Mallick, and S. Jha, *Sci. Rep.* 5, 14813 (2015).
49. C.C. Berry, S. Wells, S. Charles, and A.S. Curtis, *Biomaterials* 24, 4551 (2003).
50. N. Beyth, Y. Hourri-Haddad, A. Domb, W. Khan, and R. Hazan, *Evid. Based Complement. Altern. Med.* 2015, 246012 (2015).
51. A.A.H. El-Bassuony and H.K. Abdelsalam, *J. Mater. Sci. Mater. Electron.* 31, 3662 (2020).
52. M.A. Sayed, H.K. Abdelsalam, and A.A.H. El-Bassuony, *World J. Microbiol. Biotechnol.* 36, 25 (2020).
53. M.A. Sayed, A.A.H. El-Bassuony, and H.K. Abdelsalam, *Braz. J. Microbiol.* 51, 1475 (2020).

Publisher's Note Springer Nature remains neutral with regard to jurisdictional claims in published maps and institutional affiliations.